Proceedings of the 21st ICSMGE, Vienna, Austria, 14 – 19 June 2026. Pistrol, Adam & Schweiger (eds.)
Published by: ÖGG, Austrian Society for Geomechanics, Salzburg, Austria, ISBN 978-3-9503898-4-5
https://doi.org/10.53243/ICSMGE2026-1100

Adaptation of direct shear equipment to perform tests under constant stiffness conditions on natural, artificial and treated geotechnical interfaces

Alvaro Boiero, Enrique Romero, Marcos Arroyo, Fernando Sossa
Universitat Politècnica de Catalunya - Barcelona-TECH, and International Centre for Numerical Methods in Engineering CIMNE, Spain, alvaro.boiero@upc.edu

Giovanni Spagnoli
Sweco GmbH, Germany

ABSTRACT: A constant normal stiffness condition is representative of many *in situ* processes of shear deformation close to geotechnical interfaces, for instance, those occurring alongside tree roots when trees are uprooted from the soil or close to the wall of a pile when the pile is axially displaced. Those pile-soil interfaces are sometimes improved using binders to enhance axial pile capacity. A direct shear test device was adapted to shear soil and soil-structure interfaces under constant stiffness conditions. The apparatus-specific adaptations also allowed the injection of binders into the soil specimen to simulate binder permeation under stress conditions similar to those that could occur in the field. This paper describes the adaptations made to the original direct shear apparatus and the calibrations performed to ensure reliable measurements, before illustrating the apparatus performance with results obtained in tests of sand-root and colloidal silica improved sand-steel interfaces.

KEYWORDS: Direct shear test, constant stiffness conditions, interface direct shear test, colloidal silica, soil-pile interface.

1 INTRODUCTION

The mechanical behaviour at interfaces has a crucial influence on the overall performance of many geotechnical structures. The classical method for quantifying strength at interfaces has involved the use of direct shear equipment (typically to obtain peak and -in some cases- critical state shear strength) or torsional direct shear devices (which allow residual strength conditions to be achieved). In both types of equipment, a constant normal load is usually applied to the interface, while the behavior under a constant shear load or shear or displacement rates is observed. In these conditions, shear occurs under the action of a constant normal load (CNL), and this kind of stress-controlled test is representative, for instance, of conditions relevant to most slope failure surfaces.

However, there are certain practical cases in which the normal stress acting at the interface could be variable during the shearing process: if dilation or contraction of the material accompanies the movement while displacement of the soil (or rock) normal to the interface is constrained in some way, then the normal stress may change during shearing. In these cases, it may be unrealistic to model the behaviour of the interface in the laboratory under CNL conditions (Ooi & Carter, 1987).

A particular case of confined contraction/dilation is given by the conditions associated with a soil-pile interface when the pile is subjected to service loads. Essentially, the shear resistance at the soil-pile interface can be modelled based on the Mohr-Coulomb failure criterion, as expressed by the following equation:

$$\tau_s = (\sigma'_{ro} + \Delta\sigma'_r) \tan \delta' \qquad (1)$$

The effective radial stress σ'_r depends mainly on the horizontal stress at rest σ'_{ro} and a dilatancy component $\Delta\sigma'_r$, generated during pile loading and constrained by the stiffness of the surrounding soil (Wernick, 1978; Ooi & Carter 1987; Jardine et al., 1993, 2005; Porcino et al., 2003). This mechanism can be reproduced in the laboratory using the direct shear test under constant normal stiffness conditions (DST$_{(CNS)}$), as shown in Figure 1. This figure illustrates the mobilisation mechanism along the pile shaft under axial compressive loading, including a schematic of the laboratory simulation using the DST$_{(CNS)}$ test.

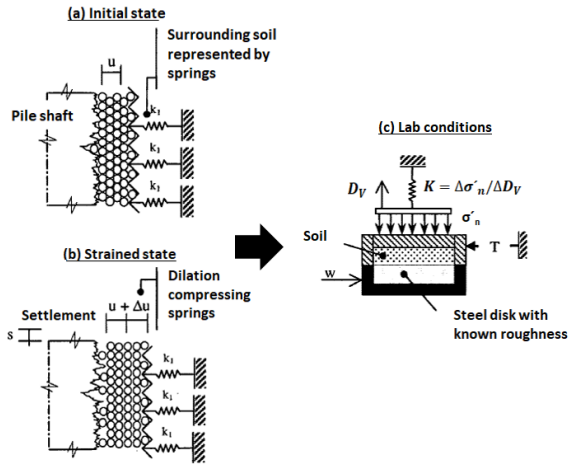

Figure 1. Loaded pile-soil interface behavior reproduced by DST$_{(CNS)}$ in the laboratory.

For drained shear stress conditions under constant normal stiffness (CNS), changes in effective normal stress at the interface are expressed as:

$$\Delta\sigma'_n - \Delta D_v \, K = 0 \qquad (2)$$

where $\Delta\sigma'_n$ is the effective normal stress increment acting on the shear plane, ΔD_v is the interface height variation associated with a contraction or dilation mechanism (equivalent to Δu in the pile schematics (a) and (b) of the figure), and K is the constant normal stiffness of the system, ideally representing the lateral stiffness of the soil surrounding the pile. Such lateral stiffness K is traditionally estimated using cylindrical cavity expansion theory (Lehane et al, 2022). For elastic isotropic materials, this suggests that K is directly proportional to the shear modulus of the soil and inversely proportional to the pile diameter.

This work describes the adaptation of a conventional direct shear apparatus to perform DST$_{(CNS)}$ tests on soil and interfaces, including interfaces treated with binders injected along the interface under normal stress. In addition, the protocol developed to measure the vertical displacements of the specimen before and during shearing is depicted, and typical

results obtained in tests performed to study the behavior of several soil-material interfaces are presented.

2 ADAPTATIONS ON THE DST APPARATUS

Figure 2 illustrates the characteristics of the original direct shear equipment and the adaptations made in it to simulate CNS conditions.

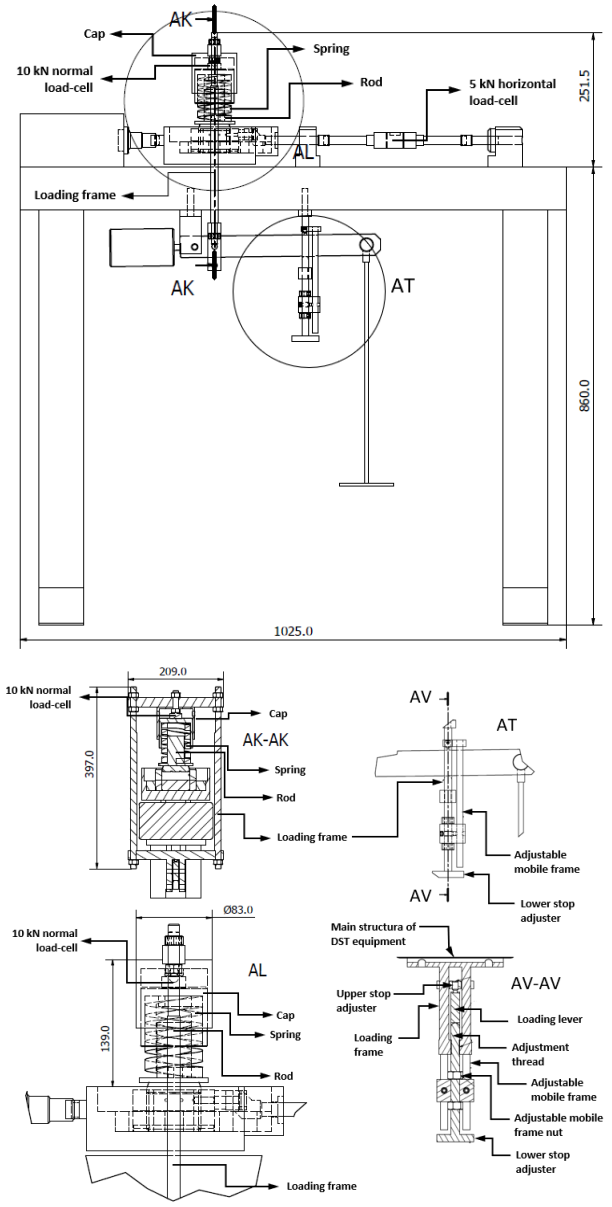

Figure 2. Schematics of the DST_{CNS} adapted equipment (dimensions in millimeters).

The adaptations were carried out on a Wykeham Farrance model 27-WF2160 AUTOSHEAR direct shear apparatus, similar to direct shear equipment commonly available in commercial and research laboratories around the world. As shown in Figure 2, the CNS state is achieved using a spring with a known elastic constant (K_{spring}), a rod with a base diameter of 60 mm (matching the sample diameter), and a cap that protects and connects the spring to the loading frame. Additionally, a 10 kN HBM C9C load cell was installed to measure the variations in the normal force applied to the specimen during the test (see cross-section AK-AK and detail AL in Figure 2).

The vertical and horizontal displacements of the specimen are recorded by LVDT sensors located at the top of the loading frame and in the lower section of the shear box, respectively; while a 5 kN horizontal load cell records the shear force using data acquisition software integrated into the direct shear apparatus. The pre-shear initial normal stress σ'_{no} is established through an adjustable mobile frame, which fixes the original lever arm and allows the spring to be connected to the movement of the sample during shearing (see detail AT and cross-section AV-AV in Figure 2).

This arrangement allows capturing equation (2) above: when the sample (improved or not) dilates, there is an increase in the value of D_v and, under a constant stiffness K, a consequent increase in the normal stress σ'_n; when the sample contracts, the opposite effect occurs.

The load cell installed at the top of the spring records the variation of the normal force acting on the sample. Hooke's law allows redundant validation of the force based on the recorded sample height variation and the spring constant.

For testing improved soil-pile interfaces, a separate modification of the shear box was carried out to simulate the *in-situ* injection process. Such a modified box includes holes for the inlet of the binder and for the outlet of the water present in the voids of the sample, displaced by the binder injected under pressure. Figure 3 shows a schematic of the shear box, illustrating the positions of the inlet and outlet holes.

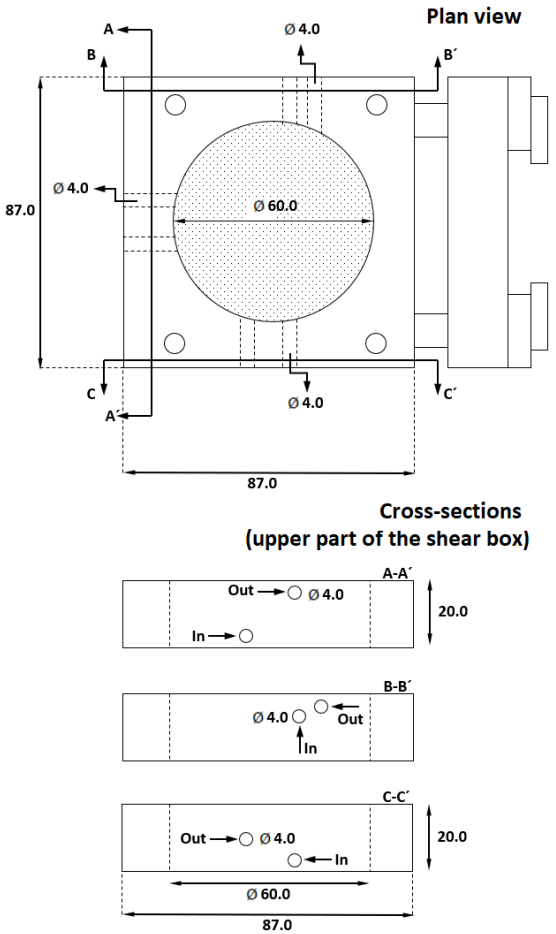

Figure 3. Schematics of the adapted direct shear box, as well as inlet and outlet holes (dimensions in millimeters).

3 MEASUREMENT OF VERTICAL DISPLACEMENT

In principle, the vertical displacement of the specimen D_v can be inferred either from the displacement measured through the

LVDT device placed at the top of the load frame or from the force recorded with the load cell, related to vertical displacements through the spring constant. However, it was necessary to overcome several practical difficulties to obtain reliable measurements.

3.1.1 *Vertical displacement during preloading*

Due to the external position of the LVDT (Figure 4), the vertical displacement measured by this instrument also includes contributions from vertical displacements originating, for instance, from bulk displacements of the elements that make up the system, from imperfections on contact surfaces, or from adjustments in bolted connections between different equipment parts. These parasitic vertical displacements also affect the loading spring response. Parasitic vertical displacements may nevertheless be corrected after calibration.

For this purpose, the test system can be simplified as a set of series-connected springs (see Figure 4), representing the main elements of the system susceptible to displacements during the test. In the figure, spring A represents a subsystem consisting of the loading spring, rod, and cap. In contrast, spring B represents a subsystem including the shear box, porous stones and, when testing interfaces, the block of material interfacing with the soil (steel, wood, etc.). Displacements of the load cell are not included, since its stiffness is several orders of magnitude greater than that of all the other system components.

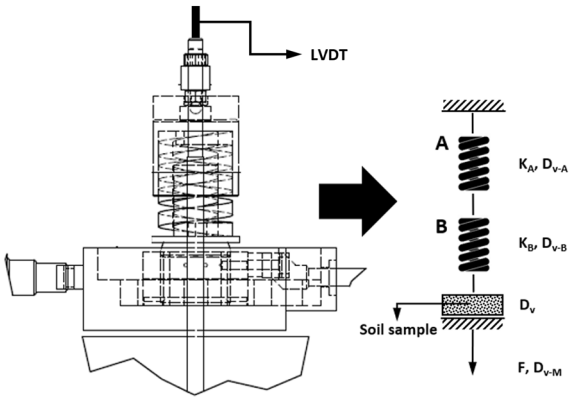

Figure 4. Simplified system as two springs in series.

From Figure 4, when the system is subjected to an initial force F_o, the total displacement of the system recorded on the LVDT placed at the top of the loading frame, D_{v-M}, can be considered as the sum of the displacements of subsystems A and B, plus the displacement of the specimen:

$$D_{v-M} = D_{v-A} + D_{v-B} + D_v \tag{3}$$

Equation (3) can be expressed as a function of the normal stress $\sigma'_n=F/A$ (where A is the cross-sectional area of the specimen) and the stiffnesses K_A and K_B, and rearranged to obtain the specimen deformation D_v.

$$D_v = D_{v-M} - \frac{\sigma'_n}{K_A} - \frac{\sigma'_n}{K_B} \tag{4}$$

This equation allows for obtaining the initial displacement of the specimen once the system-linked stiffnesses K_A and K_B are determined. To determine K_A, vertical loads are applied to the system without the shear box. To determine K_B, vertical loads are once again applied to the system, now including a shear box with all its internal components (porous stones, interface material, etc.), but without a soil specimen or the parts of subsystem A. Examples of these calibration measurements are discussed below in section 4.

3.1.2 *Vertical displacement during shearing*

A shear box may tilt or rotate slightly during shearing (Jewell, 1989; Lings & Dietz, 2004). Given the test configuration, that motion will be amplified by the presence of the cap housing the spring. As a result, the LVDT measurements at the top of the cap ceased to be a reliable indicator of vertical sample displacement, even if vertical system compliance was corrected as in the previous section.

An alternative was found exploiting the load cell measurements, which, in principle, were less sensitive to any slight tilting problem. Indeed, if the variation of the displacement with respect to the initial value of the specimen, ΔD_v, and the variation of the stress with respect to the initial one, $\Delta\sigma'_n$, are known, it is possible to apply equation (2) assuming an effective stiffness K_{eff} to estimate the evolution of the vertical sample displacement during the test.

Using the measured normal stress $\sigma'_n=F/A$, the sample displacement is determined as follows:

$$D_v = \frac{\sigma'_n}{K_{eff}} \tag{5}$$

where K_{eff} is an effective system stiffness determined by considering the stiffness of springs A and B in series (see Figure 4):

$$K_{eff} = \frac{K_A K_B}{K_A + K_B} \tag{6}$$

4 EXAMPLES OF INTERFACE TESTING RESULTS

To illustrate the use of the shearing equipment adapted for testing under CNS conditions, this section shows some results obtained in soil-root, sand-steel, and sand-injected steel interface tests. The properties of the materials (roots, soils, steel, binders) are reported elsewhere (Boiero et al 2024a and 2024b).

The first step in performing this type of test is to determine the effective stiffness of the test system, K_{eff}. For this, it was necessary to determine the stiffnesses of the subsystems K_A and K_B as indicated in Figure 4. These stiffnesses are obtained from the slope of the ratio between the normal stress, σ_n, and the normal displacement, δ_n, measured in normal load-controlled tests performed for each subsystem in the shear equipment. Figure 5 shows the curves obtained for subsystem A (considering two different reaction springs of varying constants) and for subsystem B (considering two interfaces, one of steel and the other of wood).

As indicated in Figure 5, for a constant spring K_{spring}=0.507 kN/mm, K_A=158 kPa/mm, while for a spring with K_{spring}=0.819 kN/mm, K_A=178 kPa/mm. For the case of subsystem B, K_B was determined as the secant stiffness for the load intervals relevant for the interface tests, resulting in K_B=3835 kPa/mm for the interface with steel and K_B=117 kPa/mm for the interface with wood. It is evident that the higher the reaction spring stiffness is, the higher the stiffness of subsystem A will be. Likewise, subsystem B stiffness is strongly influenced by the stiffness of the interface material.

Table 1 summarizes the main characteristics and component stiffness values calibrated for the different DST(CNS) tests performed.

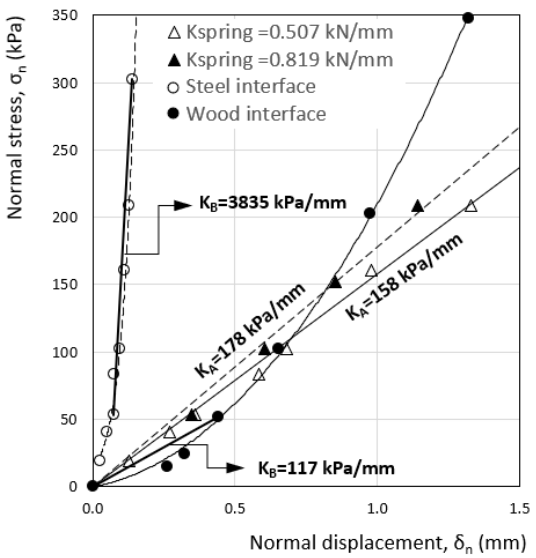

Figure 5. Results of normal loading tests and stiffnesses of sub-systems A and B.

Table 1. Component stiffnesses for different systems in interface $DST_{(CNS)}$ tests.

Interface	K_A (kPa/mm)	K_B (kPa/mm)	K_{eff} (kPa/mm)
Sand-steel	158	3835	152
Improved sand-steel(*)	178	3835	170
Sand-real root(**)	158	117	67

(*) Sand was improved by an acrylate grout (Boiero *et al*, 2024a).
(**) Real root from Pinus halapencis (Boiero *et al*, 2024b).

Figures 6, 7, 8 and 9 show the evolution of shear stress τ, stress ratio τ/σ'_n, vertical displacement D_v, and effective normal stress σ'_n, respectively, with horizontal displacement D_H, obtained in some representative tests. Figure 10, on the other hand, records the variation of the effective normal stress $\Delta\sigma'_n$ with respect to the variation of the normal vertical displacement ΔD_v, which is equivalent to plotting K_{eff} from equation (5).

It is important to note that the normal stresses applied to test the sand-steel interfaces were considerably higher (of the order of 100 kPa to 200 kPa) than those used when testing the soil-root interfaces (around 25 kPa). This is related to the different stresses that are relevant in soil-pile and soil-root interactions and illustrates the broad scope of applicability of the modified apparatus. On the other hand, as can be seen in Figure 7, the soil-root interface, although it worked under lower normal stress, achieves the highest normalized strength, indicating high frictional efficiency, attributable to its high roughness and mechanical interlocking. However, after the peak, it shows a marked softening, possibly due to soil reorganization around the irregular geometry of the root. In contrast, the sand-steel and injected sand-steel interfaces, subjected to higher normal stresses, exhibit more stable and frictional behavior, with lower τ/σ'_n values, although chemical improvement does increase the frictional strength. The similarity in shape between the two sand-steel curves indicates that natural root roughness mainly influences the phenomenon beyond just chemical adhesion and simple friction with steel. Therefore, roughness is a key factor in the maximum strength, although its influence is affected by confinement and contact stability as the interface gradually deforms.

Figures 8, 9 and 10 show the behavior of the interface under CNS conditions. Figure 8 shows that, in general, the behavior of the tested interfaces is dilatant, while Figure 9 shows a tendency to increase the effective normal stress during shear. Both trends agree with equation (2), whose graphical representation for each of the tests is shown in Figure 10.

In addition, regarding Figure 10, the influence of the stiffness of the interface materials is evident, as mentioned above: the effective stiffness of the sand-steel interfaces is between 2.2 and 2.5 times the effective stiffness of the soil-root interface.

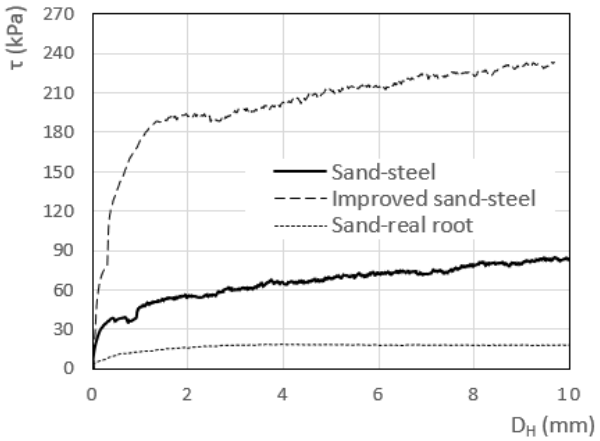

Figure 6. Shear stress versus horizontal displacement from $DST_{(CNS)}$.

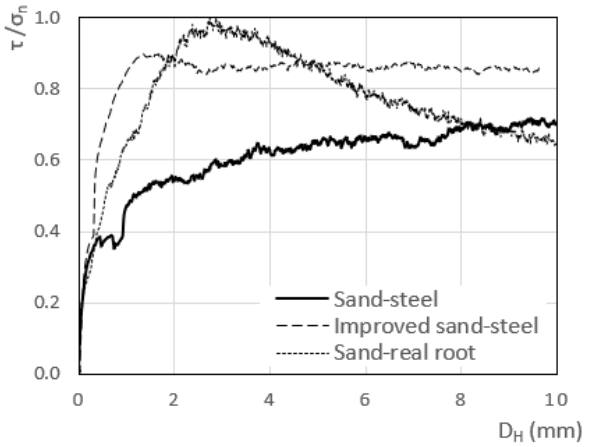

Figure 7. Stress ratio versus horizontal displacement from $DST_{(CNS)}$.

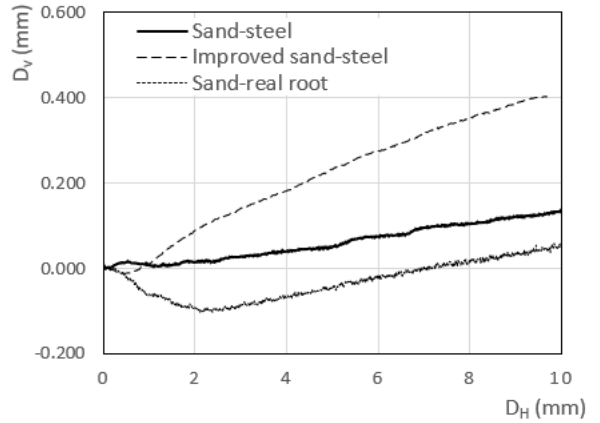

Figure 8. Vertical displacement versus horizontal displacement from $DST_{(CNS)}$.

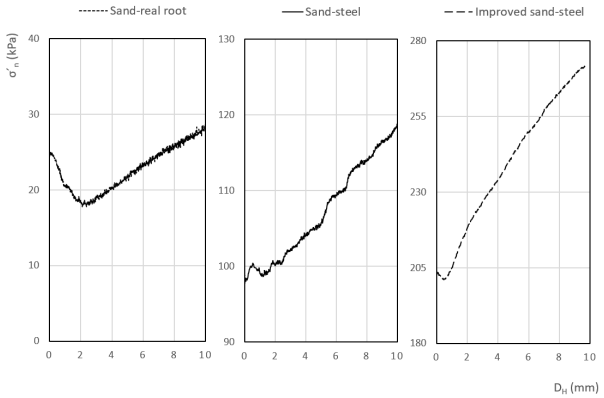

Figure 9. Effective normal stress versus horizontal displacement from $DST_{(CNS)}$.

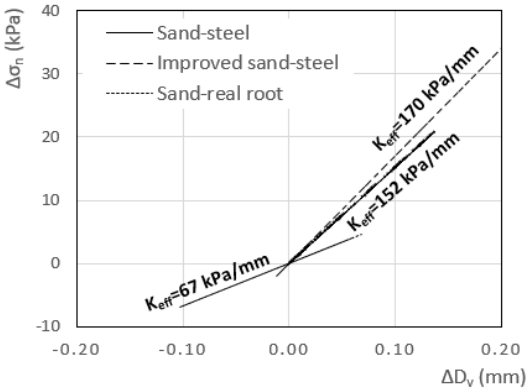

Figure 10. Variation of effective normal stress versus variation of vertical displacement from $DST_{(CNS)}$.

5 STRESS-DILATANCY

Stress-dilatancy relations offer a consistent framework for direct shear and interface shear test interpretation (Dove & Jarret, 2002; Dietz & Lings, 2006). The behaviour of a sand-steel interface was examined within the stress-dilatancy framework to confirm the robustness of the testing and calibration protocols developed for $DST_{(CNS)}$ tests with the adapted equipment.

In classical soil mechanics, several flow rules have been proposed to explain the dilatant behavior of granular soils (Taylor, 1948; Rowe, 1962; Bolton, 1986). For the case of Ottawa sand-steel interfaces, Dove & Jarret (2002) report a good agreement between measured and predicted peak friction angles using Bolton's (1986) criterion and demonstrate that: 1) critical state concepts apply to interface systems; and 2) roughness controls dilation, which, in turn, controls strength. On the other hand, Dietz & Lings (2006) proposed the use of Taylor's (1948) rule modified for interfaces, which can be written as follows:

$$\tan \delta'_p = \tan \delta'_{ld} + \tan \alpha \quad (5)$$

where δ'_p is the peak friction angle at the interface, δ'_{ld} is the critical state friction angle at the interface corresponding to large displacements, and α is the dilatancy angle. This dilatancy angle α is calculated as:

$$\tan \alpha = \frac{D_v}{D_H} \quad (6)$$

The measurements acquired during three $DST_{(CNS)}$ tests on sand-steel interfaces, treated with colloidal silica or untreated, are here analyzed considering the approach proposed by Dietz & Lings (2006). Table 2 summarizes the data associated with each test (Dr_0 represents the starting relative density). For the three tests, an initial effective normal stress σ'_{no}=200 kPa was considered. One test was performed using silica sand in its natural state. Two other tests were done on the same sand after permeation with colloidal silica suspensions of 15% and 40% silica concentration, respectively. In these three tests, a steel disc with constant roughness R_t=26 μm was placed at the bottom of the shear box. The tests were performed at the same effective stiffness. More details about the characteristics of the materials employed may be found in Boiero et al (2024a).

Table 2. Performed interface $DST_{(CNS)}$ for validation.

Interface	Dr_o	σ'_{no} (kPa)	σ'_{nf} (kPa)	K_{eff} (kPa/mm)
Sand-steel	0.759	200	251	170
Sand(15%CS)-steel	0.754	200	266	170
Sand(40%CS)-steel	0.755	200	285	170

Figures 11 and 12 show the evolution of shear stress τ and stress ratio τ/σ'_n with horizontal displacement D_H. From Figure 12, the values of δ'_p and δ'_{ld} were derived, and subsequently the value of the dilatancy angle α was estimated for each test based on equation (7).

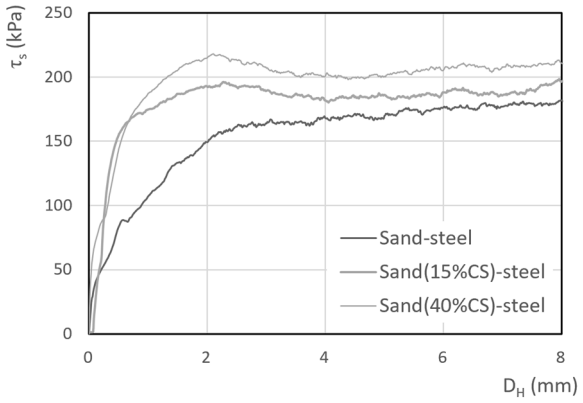

Figure 11. Shear stress versus horizontal displacement from $DST_{(CNS)}$.

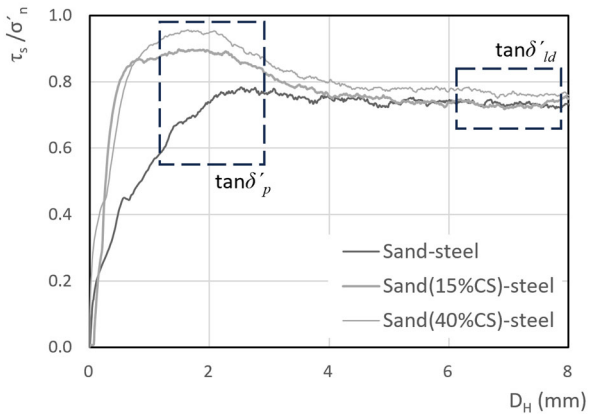

Figure 12. Stress ratio versus horizontal displacement from $DST_{(CNS)}$.

The sand enhanced with CS composites presents an adhesion component. This means that the interface behavior is characterized by the simultaneous presence of two shear-resistant mechanisms: adhesion, associated with the physical-chemical interaction between the CS and the steel surface, and friction mobilized during relative sliding. It is assumed that

during the initial stages of displacement, i.e., before the peak, both mechanisms contribute to shear resistance. From that point onwards, the system may experience a partial loss of adhesion and a change in the frictional response. Analyzing a broader campaign on CS treated steel interfaces, it was concluded (Boiero et al, 2024a) that the adhesion strength component was of the order of 10% to 15% of τ. Thus, for sands improved with CS:

$$\frac{\tau - c_{ad}}{\sigma'_n} \approx \beta \frac{\tau}{\sigma'_n} \quad (7)$$

where c_{ad} is the adhesion strength component. Using the adhesion ratios mentioned above leads to $\beta \approx 0.85$-0.90 for the interfaces studied.

Figure 13 shows the evolution of the vertical displacement D_v as a function of D_H for the interfaces studied. The dilatancy observed is in good agreement with the limiting values that are derived from Taylor's expression (equation 7) using the peak and critical state friction angles derived from the shear stress plot. The good coincidence that is observed between the deduced dilatancy value and the measurements may be seen as evidence that the modified test apparatus and applied measurement correction protocols are performing well.

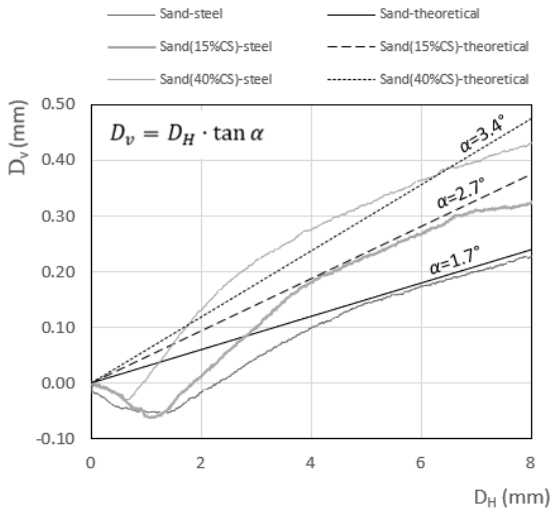

Figure 13. Vertical displacement versus horizontal displacement from $DST_{(CNS)}$. Analysis of dilatant behavior (Taylor's rule).

6 CONCLUSIONS

The modifications to the direct shear equipment for conducting tests under constant normal stiffness conditions have been outlined. These changes are relatively simple and can be implemented in any standard direct shear apparatus at a moderate cost. Measurement correction protocols have been provided for vertical displacements under vertical loading and during shearing, considering the different test systems' stiffnesses involved in the measurement. Measurements corrected according to the developed testing protocols show good agreement with the expected theoretical values based on dilatancy angle, for interface tests with natural soils and improved materials. In this regard, it is worth noting that the adapted shear box enables the simulation of injection processes under *in situ* stress conditions, which is very useful for analyzing the strength of soils and interfaces between materials and improved soils.

7 ACKNOWLEDGMENT

The authors are grateful for the financial support provided by MCIN/AEI/10.13039/501100011033 and the European Union Next Generation Fund EU/PRTR.

8 REFERENCES

Boiero, A., Romero, E., Arroyo, M., and Spagnoli, G. 2024a. Interface direct shear tests with novel binders. *7th International Conference on Geotechnical and Geophysical Site Characterization*, Barcelona. DOI: 10.23967/isc.2024.012.

Boiero, A., Arroyo, M., and Romero, E. 2024b. Physical models of mechanical root-soil interaction. *Proceedings of the XVIII ECSMGE 2024*, Lisboa, 1-6. DOI: 10.1201/9781003431749-550.

Bolton, M.D. 1986. The strength and dilatancy of sands. *Géotechnique* 36(1), 65-78.

Dietz, M.S., and Lings, M.L. 2006. Postpeak strength of interfaces in a stress-dilatancy framework. *Journal of Geotechnical and Geoenvironmental Engineering* 132(11), 1474-1484.

Dove, J.E., and Jarret, J.B. 2002. Behavior of dilative sand interfaces in geotribology framework. *Journal of Geotechnical and Geoenvironmental Engineering* 128(1), 25-37.

Jardine R., Lehane B., and Everton, S. 1993. Friction coefficients for piles in sands and silts. *Offshore Site Investigations and Foundations Behaviour* 28, 661-677.

Jardine R., Chow F., Overy, R., and Standing, J. 2005. ICP design methods for driven piles in sands and clays. Thomas Telford. London, UK.

Jewell, R. A. "Direct shear tests on sand." *Geotechnique* 39.2 (1989): 309-322.

Lehane, BM., Bittar, E.J., Lacasse, S., Liu, Z., and Nadim, F. 2022. New CPT method for evaluation of the axial capacity of driven piles. *Cone Penetration Testing 2022*, 3-15. DOI: 10.1201/9781003308829-1.

Lings, M. L., & Dietz, M. S. (2004). An improved direct shear apparatus for sand. Géotechnique, 54(4), 245-256.

Ooi, L.H., and Carter, J.P. 1987. A constant normal stiffness direct shear device for static and cyclic loading. *Geotechnical Testing Journal* 10(1), 3-12.

Porcino, D., Fioravante, V., Ghionna, V., and Pedroni, S. 2003. Interface behavior of sands from constant normal stiffness direct shear tests. *Geotechnical Testing Journal*, Vol. 26, No. 3.

Rowe, P. 1962. The stress-dilatancy relation for static equilibrium of an assembly of particles in contact. *Proceedings of the Royal Society, Series A* 269, 500-527.

Taylor, D. 1948. Fundamental of Soil Mechanics. Jonh Wiley & Sons, New York, USA.

Uesugi, M., Kishida, H., and Tusbakihara, Y. 1988. Behavior of sand particles in sand-steel friction. *Soils and Foundations* 28(1), 107-118.

Wernick, E. 1978. Stress and strains on the surface of anchors. *Rev. Fr. Géotech.* (3), 113–119.